Probing the Molecular and Electronic Structure of Norhipposudoric and Hipposudoric Acids from the Red Sweat of *Hippopotamus amphibius*: A DFT Investigation

Vinicio Galasso

Dipartimento di Scienze Chimiche, Università di Trieste, I-34127 Trieste, Italy

Fabio Pichierri*

G-COE Laboratory, Department of Applied Chemistry, Graduate School of Engineering, Tohoku University, Aoba-yama 6-6-07, Sendai 980-8579, Japan

Received: October 15, 2008; Revised Manuscript Received: January 8, 2009

Molecular structure and tautomeric/conformational preferences of norhipposudoric and hipposudoric acids, the recently isolated pigments of the *Hippopotamus amphibius*' sweat, were investigated using the density functional theory (DFT) PBE0 formalism. Among a large variety of possible structures, two similar keto−enol tautomer/conformers are nearly isoenergetic and markedly more stable than the others both in the gas phase and aqueous solution. The bulk solvent effect was accounted for with the polarizable continuum model (PCM). A distinctive structural feature is the strong intramolecular hydrogen bonding in the keto−enol O−H···O bridge, as shown by analysis of the atoms-in-molecules topological properties of the electron density. To elucidate the claimed strong acidity of these pigments, the site-specific microscopic dissociation constants were also calculated using the cluster-continuum model, a hybrid approach based on inclusion of explicit solvent molecules and solvation of the cluster by the dielectric continuum. Notably, the first deprotonation should occur predominantly from the enolic group with a remarkably low pk_i value. This factor could play an important role in the potent antibiotic activity of the pigments. The absorption spectra of the undissociated and dissociated compounds in aqueous solution were interpreted with time-dependent DFT/PCM calculations. The $\pi-\pi^*$ diquinoid excitations, mainly occurring in the fluorenoid nucleus, are the major contributors to the color and strong absorption bands in the UVA and UVB regions, which are closely related to the efficient sunscreen activity exerted by the pigments.

1. Introduction

A team of Japanese researchers led by Kimiko Hashimoto have recently succeeded in collecting enough samples of the *Hippopotamus amphibius*' sweat to isolate and characterize the two compounds mainly responsible for the colorful reaction observed on the hippopotamus's skin.[1] (The colorless secretion over the entire hairless body turns red within a few minutes and then gradually brown after a few hours as the pigments polymerize.) Thus, they have overthrown the ancient, popular myth that the "hippopotamus sweats blood". In the pachyderm, these natural pigments are produced from skin glands.[2] By using the Pschorr reaction, the Japanese researchers have also been successful in the synthesis of these two highly unstable pigments and named them "norhipposudoric acid" (**NH**; orange pigment) and "hipposudoric acid" (**HP**; red pigment) (Figure 1).[3−5]

A noteworthy point is that these tricyclic compounds, incorporating a fluorenoid nucleus, are endowed with outstanding biochemical properties. The mixture of these strongly acidic compounds, far more powerful than vinegar, indeed acts as an effective sunscreen and antibiotic.[1−5] First, it keeps the hippopotamus cool and protects him from the harmful effects of solar radiation. Second, it defends the hippopotamus, a belligerent animal often subject to serious wounds, from certain pathogens and accelerates the recovery.

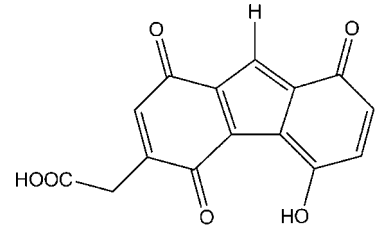

NH

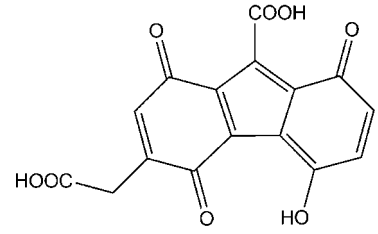

HP

Figure 1. Molecular formulas of pigments **NH** and **HP**.

Despite the importance of such a discovery, no quantum-mechanical investigation has been devoted to these compounds so far. Therefore, it was considered timely to extract some important information on the molecular and electronic structures of these molecules by employing density functional theory (DFT) methods and comparing the results with the available

* To whom correspondence should be addressed. E-mail: fabio@che.tohoku.ac.jp.

10.1021/jp809138s CCC: $40.75
Published on Web 02/24/2009

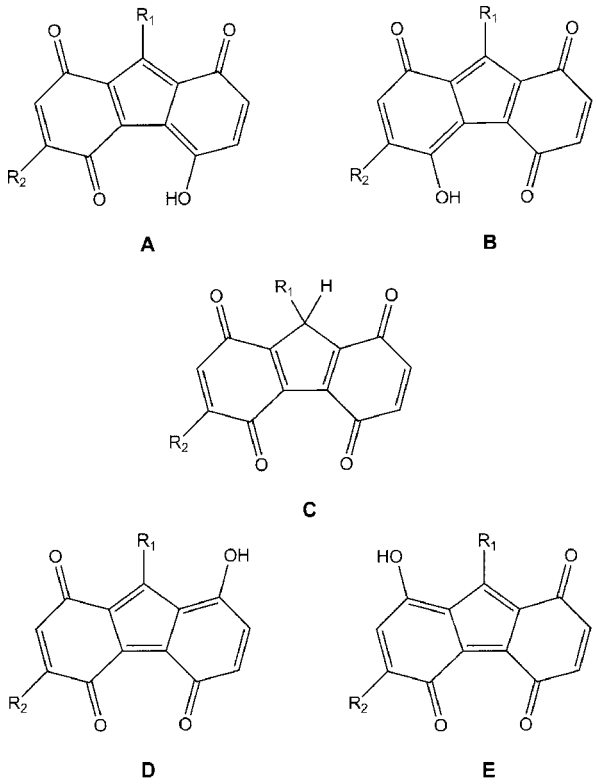

Figure 2. Possible tautomers of pigments **NH** (R_1 = H, R_2 = CH_2COOH) and **HP** (R_1 = COOH, R_2 = CH_2COOH).

experimental data. Thus, among the various possible tautomers (Figure 2), the most favorable conformers of both the neutral and anionic species have been found. In particular, the remarkable pattern of their hydrogen bonds has been characterized on a topological basis. Furthermore, the computation of the acid dissociation constants confirms the relative acidity strength and shows the favored ionization pathway in these diprotic (**NH**) and triprotic (**HP**) acids. Last, the electronic transitions, computed at a time-dependent (TD)-DFT level, provide a rational interpretation of the broad absorption in the UVA and UVB regions of the spectrum, so of the sunscreen activity.

2. Computational Details

The molecular structures of all the **NH** and **HP** species in the gas phase were studied with the parameter-free DFT/PBE0 hybrid functional[6] by using the 6−311+G(d,p) basis set. Harmonic frequency calculations were performed for all the optimized structures to establish that the stationary points are local minima on the corresponding potential energy surfaces.

Vertical $S_n \leftarrow S_o$ excitation energies and oscillator strengths were calculated with the (time-dependent) TD-DFT method,[7] employing the PBE0 functional and the 6−311+G(d,p) basis set and accounting for the bulk solvent effects with the polarizable continuum model (PCM).[8]

All of these calculations were carried out with the Gaussian-03 package of programs,[9] except those for the topological properties of the electron density that were performed with a local program.

3. Results and Discussion

A. Structural Properties. ***1. Conformational Preferences.*** The hippopotamus' natural pigments **NH** and **HP** show a complex structural pattern. Indeed, they can exist as a mixture of five tautomers, as shown in Figure 2, the keto−enol species A, B, D, and E and the bisquinoid species C. Their molecular shape can be described as a dish, the fluorenoid nucleus, provided with a flexible carboxymethyl group and a further carboxylic unit in the **HP** case. Thus, **NH** and **HP** have three and five main torsion angles, respectively (see scheme below Table 1), that give rise to a large number of conformational isomers. This structural pattern becomes still more complicated in solution, where **NH** and **HP** can exist in neutral, anionic, and dianionic (also trianionic in the **HP** case) forms, making their spectroscopic properties strongly dependent on pH and environment.

The DFT values of the torsion angles and the energies relative to the most stable tautomer/conformers in the gas phase are reported in Table 1. Figure 3 shows the DFT lowest-energy tautomer/conformers of the neutral and anionic forms of **NH**. The DFT lowest-energy structures of the neutral and anionic forms of **HP** are depicted in Figures 4 and 5.

A cursory survey of the most relevant structural aspects prompts the following remarks:

(i) Common to the preferred conformers of all the tautomers A−E is that the carboxymethyl group is twisted by ca. 70° to the approximately planar fluorenoid moiety and has a *syn*-COOH arrangement, as observed experimentally for the simple parent compounds phenylacetic acid[10] and homogentisic acid.[11] This situation is denoted with label nhb (non-hydrogen-bonded carboxymethyl group) in Table 1.

(ii) Among the various tautomers, the most stable are tautomers A and B, which are stabilized by the strong intramolecular hydrogen bond >C═O···HO−, connecting the enol group with the proximate ketonic oxygen. These two tautomers have similar electric dipole moments (see Table 1).

(iii) The bisquinoid tautomer C is strongly disfavored by some 20 kcal mol^{-1} relative to A and B. Therefore, it is expected to be absent in the possible tautomeric mixture.

(iv) Also the tautomeric forms D and E are remarkably less stable than A and B in the gas phase. The energy gap is less in **HP** than in **NH**. In **HP**, the stabilization stems from the central carboxylic group that extends π-conjugation of the fluorenoid moiety and forms a hydrogen bond with the neighbor ketonic oxygen.

(v) According to DFT, the global minimum structure corresponds to tautomer A, which is preferred by 0.8 and 1.1 kcal mol^{-1} over tautomer B in **NH** and **HP**, respectively, in the gas phase. Notably, the A ↔ B interconversion occurs through a low energy barrier for proton transfer of 1.6 and 1.4 kcal mol^{-1} for **NH** and **HP**, respectively (as determined with the synchronous transit-guided quasi-Newton method, STQN/QST2 variant[12]). Furthermore, for both **NH** and **HP**, the energy difference between A and B is reduced to 0.5−0.7 kcal mol^{-1} in aqueous solution. On this basis, as concerns the neutral species, one may speculate that a mixture of the two most stable tautomers A and B exists at room temperature in the gas phase and solution, with a predominant amount of A and negligible presence of tautomers C−E.

(vi) For all the tautomers A−E, the conformational isomer with the carboxymethyl group in anti arrangement and twisted to form an hydrogen bond with the neighbor carbonyl oxygen, denoted with label hb (hydrogen-bonded acetyl group) in Table 1, is predicted to be higher in energy compared to the unbonded syn side chain by 2.2 and 3.3 kcal mol^{-1} in the case of **NH** and **HP**, respectively. The repulsive steric factors weaken the stabilization effect provided by the hydrogen bond.

(vii) Concerning the various ionic species, their conformational situation is not uniform. The monoanions arising from

deprotonation of the enol group adopt the hydrogen-bonded arrangement of the side carboxymethyl group, which is favored by the net negative charge on the neighbor carbonyl oxygen. Instead, electrostatic repulsions compel both the side and central carboxymethyl anions to point away from the fluorenic moiety. The most favorable conformations assumed by all the charged species of **NH** and **HP** are reported in Table 1 and Figures 4−6.

2. Intramolecular Hydrogen Bonds. A noteworthy structural characteristic of the hippopotamus' natural pigments **NH** and **HP** concerns their intramolecular, homonuclear O−H···O hydrogen bonds (HBs). Indeed, in biological systems, HBs play a primary role in many life processes and, in particular, strong intramolecular HBs stabilize and hold the compounds in conformations suitable for binding to enzymes.[13] Also, some compounds with intramolecular HBs behave as uncouplers of oxidative phosphorylation by inhibiting the biosynthesis of adenosine triphosphate (ATP) in mitochondria.[14] In this regard, a computational characterization of the properties of the HBs in **NH** and **HP** is therefore useful to better comprehend their biological activities.

The estimation of intramolecular HB energy is much more intricate as compared to intermolecular HB. Recently, a variety of indirect theoretical methods, such as conformational analysis, the ortho-para approach, isodesmic/homodesmic reactions, partition of the energy of interactions, divide-and-conquer, atoms-in-molecules (AIM), natural bond orbital, and molecular tai-

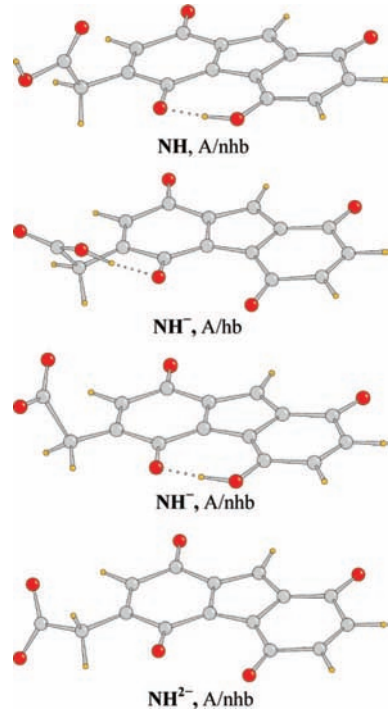

Figure 3. DFT-optimized structures of the lowest-energy tautomer/conformer of **NH** neutral and anionic species.

TABLE 1: Relative Energies (kcal mol^{-1}), Torsion Angles (deg), and Dipole Moments (Debye) of Preferred Structures in Vacuo[a]

	taut/conf[c]	ΔE	τ_1	τ_2	τ_3	τ_4	τ_5	μ
NH[b]	A/nhb	0	70.5	−170.2	−178.8			4.86
	B/nhb	0.78 (0.51)[d]	70.7	−172.5	−179.0			5.03
	C/nhb	19.82 (17.34)	70.8	−172.4	−179.8			1.56
	D/nhb	19.36 (9.44)	69.5	−164.1	−179.1			4.06
	E/nhb	16.81 (9.33)	72.3	−162.3	−179.3			5.11
	A/hb	2.18 (4.51)	76.5	−69.1	3.7			5.86
NH(ph)$^-$	A/hb	-	74.2	−60.8	4.3			
NH(cm)$^-$	A/nhb	-	105.4	−144.2				
NH^{2-}	A/nhb	-	169.5	−127.8				
HP	A/nhb	0	70.0	−171.5	−178.9	−35.2	17.4	8.68
	B/nhb	1.09 (0.65)	70.4	−174.2	−179.1	−33.1	16.1	8.97
	C/nhb	20.78(15.27)	70.4	−172.7	−179.8	57.7	−179.9	3.11
	D/nhb	5.19 (2.54)	70.0	−169.4	−179.5	−159.6	−179.1	2.47
	E/nhb	5.14 (2.49)	71.7	−161.0	−179.0	−14.7	179.0	3.38
	A/hb	3.32 (5.31)	77.3	−69.4	3.2	−35.7	17.5	8.65
HP(ph)$^-$	A/hb	-	75.5	−60.3	4.2	−33.9	17.0	
HP(cm)$^-$	B/nhb	-	106.2	−149.2		−35.2	18.1	
HP(ca)$^-$	A/hb	-	73.4	−62.2	3.9	−89.9		
HP(ph,cm)$^{2-}$	A/nhb	-	159.5	−137.8		−33.6	17.3	
HP(ph,ca)$^{2-}$	A/hb	-	70.5	−54.8	3.7	−90.2		
HP(cm,ca)$^{2-}$	A/nhb	-	123.2	−155.8		−89.7		
HP^{3-}	A/nhb	-	−178.1	−133.6		−88.9		

[a] Torsion angles: τ_1 ($C_5-C_6-C_{10'}-C_{11'}$), τ_2 ($C_6-C_{10'}-C_{11'}-O_{12'}$), τ_3 ($C_{10'}-C_{11'}-O_{12'}-H_{13'}$), τ_4 ($C_{9a}-C_9-C_{14'}-O_{15'}$), and τ_5 ($C_9-C_{14'}-O_{15'}-H_{16'}$), see scheme below. [b] Labels ph, cm, and ca correspond to phenolic, (side) carboxymethyl, and (central) carboxylic deprotonated units, respectively. [c] Tautomer/conformer; nhb and hb stand for non-hydrogen-bonded and hydrogen-bonded carboxymethyl group, respectively. [d] In aqueous solution.

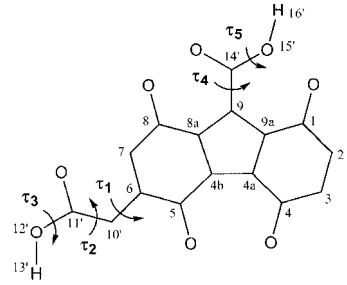

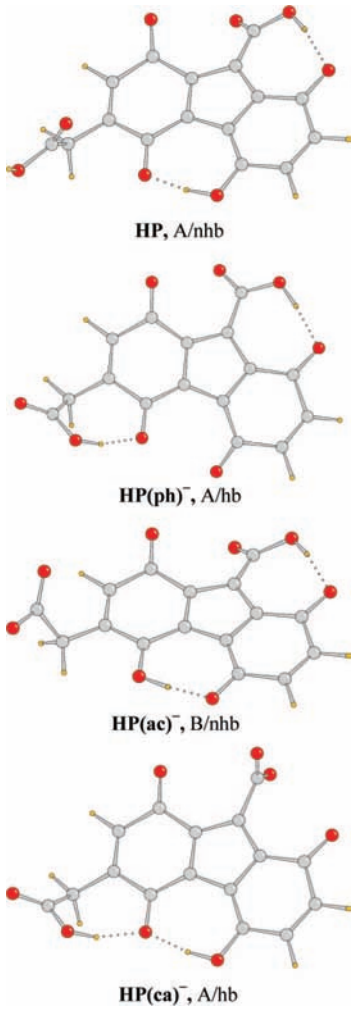

Figure 4. DFT-optimized structures of the lowest-energy tautomer/conformer of **HP** neutral and monoanionic species.

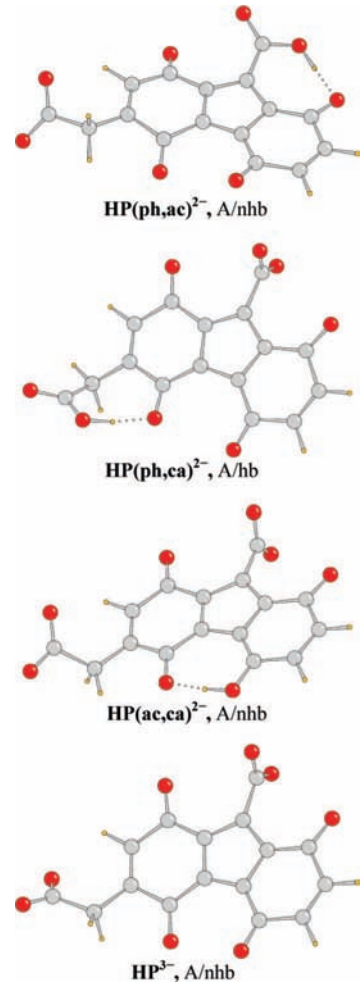

Figure 5. DFT-optimized structures of the lowest-energy tautomer/conformer of **HP** dianionic and trianionic species.

loring approaches (see refs 15−21 and references therein) have been employed to get an approximate estimation of HB energy in small- and medium-sized molecules. In particular, interatomic interactions such as HBs can be adequately described in terms of the topological properties of the electron density ρ(r) according to Bader's AIM theory of molecular structure.[22] The presence of (3,–1) ρ(r) bond critical point (BCP), where $\nabla\rho_{BCP} = 0$, characterized by a very low electron density ρ_{BCP} and a positive value of its Laplacian $\nabla^2\rho_{BCP}$, is generally considered as the manifestation of HB.[22] The AIM theory relates the topological parameters of a bond with the energy of interaction. More specifically, for closed-shell interactions such as HBs the functional of Abramov[23] relates the kinetic energy density G(r) at the BCP to the topological parameters:

$$G_{BCP} = (3/10)(3\pi^2)^{2/3}\rho_{BCP^{5/3}} + (1/6)\nabla^2\rho_{BCP} \qquad (1)$$

G(r) is in turn related to the potential energy density V(r) through the local virial theorem:

$$V_{BCP} = 1/4\nabla^2\rho_{BCP} - 2G_{BCP}$$

A simple empirical relationship between V_{BCP} and the HB energy E_{HB} has been derived by Espinosa et al.[24] from theoretical results on several molecular dimers: $E_{HB} \approx 1/2 \times V_{BCP}$. This topological approach has been followed in the present analysis.

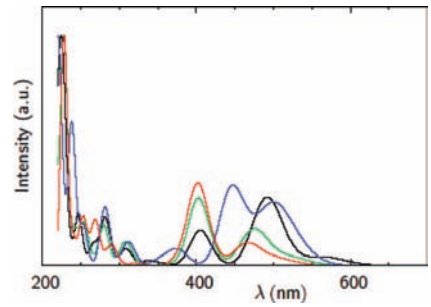

Figure 6. Computed UV−vis absorption spectra (simulated with fwhm = 0.20 eV) of **NH** species: neutral (black), enolic anion (green), carboxymethyl anion (blue), and dianion (red).

The relevant geometrical, topological, and energetic parameters in the O−H···O bridges for the most representative species of compounds **NH** and **HP** are given in Table 2. An important feature of these unsymmetrical HBs is the remarkably short H···O distance in all the **NH** and **HP** species, in particular for the keto−enol bridges. It is well-known that stronger O−H···O bonds correspond to shorter H···O contacts. Thus, if the HB becomes stronger, the O−H bond elongation is greater and the H···O and O···O distances are shorter. A parallel, consistent change is observed in the topological parameters of the electron density of the **NH** and **HP** species, whose formally π-conjugated C═O···H−O systems display HB lengths O···O varying from 2.516 to 2.771 Å. (Table 2). The properties of these H···O bondings, low ρ_{BCP} values (ranging from 0.0282 to 0.0638) and

positive $\nabla^2\rho_{BCP}$ values (ranging from 0.1171 to 0.1810), are typical for closed-shell interactions and indicate electrostatic character of the H···O bondings.[25] The estimated E_{HB} varies from −8.2 to −29.3 kcal mol^{-1}. (Of course, it must be reminded that these results may only be semiquantitative indicators and not absolute values of E_{HB}.) Thus, on an energetic basis, the relative classification of HB strength follows the decreasing order: keto−enol bridge > central carboxylic-keto bridge > side carboxymethyl-keto bridge. The strongest HB is shown by the keto−enol unit in the species **HP**/A/nhb, while the weakest HB occurs in the side carboxylic-keto fragment of the **HP**/A/hb species. Comparison of the E_{HB} values of the keto−enol bridges in the **NH** and **HP** species with the E_{HB} values reported for simpler compounds containing the C═O···H−O system, 2,4-dihydroxybut-2-ene-dial and derivatives[26] and dicoumarols,[27] as well as our estimate for the related compound juglone, i.e. 5-hydroxy-1,4-naphthoquinone (ρ_{BCP} = 0.0491, $\nabla^2\rho_{BCP}$ = 0.1417, E_{HB} = −15.6 kcal mol^{-1}), shows that the strength of some intramolecular HBs in the present molecules is remarkably high. This feature could be one of the possible factors of the effective biochemical reactivity of the hippopotamus's natural pigments **NH** and **HP**.[1] Unfortunately, lack of the experimental vibrational spectra precludes a further analysis of their HBs with references to the ν(O−H) and ν(C═O) vibrational red-shift.

In this regard, it is worthwhile noting that **NH** and **HP** should not serve as free radical scavengers. Indeed, their strong HBs cause a net increase of the bond dissociation enthalpy (BDE) of the enolic O−H bond because homolytic cleavage of such a bond involves breaking of both a covalent O−H and a hydrogen bond. Furthermore, the carboxymethyl and carboxyl groups have relatively large BDE(O−H)s. Accordingly, the DFT-computed values are 109.6 kcal mol^{-1} (enol) and 105.6 (carboxymethyl) for **NH**, and 109.0 kcal mol^{-1} (enol), 106.0 (carboxymethyl), and 104.1 (carboxyl) for **HP**. By comparison, the DFT values for simple reference compounds are 83.9 kcal mol^{-1} (phenol), 103.9 (phenylacetic acid), and 105.0 (benzoic acid). Thus, the antioxidant activity of **NH** and **HP** based on H abstractions is unlikely.

B. Acid Dissociation Constants. **NH** and **HP** are polyprotic acids. From a thermodynamic standpoint, it is possible to define a *microscopic* or *molecular* dissociation constant associated with the loss of a proton by a specific site of a polyprotic acid. Thus, referring to the first ionization step for the present cases, the possible reaction equilibria involve the enolic (microscopic dissociation constant k_e), carboxymethyl (k_a), and carboxyl (k_c) groups. The relations connecting the microscopic and *macroscopic* (experimental) constants are:[28]

$$K_1 = k_e + k_a \text{ for } \mathbf{NH}, \text{ and}$$
$$K_1 = k_e + k_a + k_c \text{ for } \mathbf{HP}$$

combined with the standard definitions:

$$pk_i = -\log k_i \text{ and } pK_{a,1} = -\log K_1$$

The first-principles prediction of accurate pK_a values in liquid phase has been an important challenging task of computational chemistry and a variety of quantum mechanical procedures have been recently reported.[29−39] For the given proton transfer reaction, the solution standard free energy (ΔG_{sol}) is expressed as the sum of the gas-phase reaction free energy (ΔG_g) and the solvation free energy (ΔG_{solv}). Commonly, the most critical point is a reasonably adequate accounting of the strong, local solute−solvent interactions.[40−45] In addition to such an aspect, the present polyprotic acids hold a variety of tautomeric/conformational forms that can be involved in deprotonation in aqueous solution. Given this structural complexity, only the acidity of the preferred conformer of the major tautomer of **NH** and **HP** was theoretically investigated here.

First, it must be remarked that preliminary pk_i calculations for **NH** and **HP** using nonsolvated species and the pure PCM method led to unsatisfactory results. Thus, the microscopic pk_is were calculated using the cluster-continuum model,[30,35,38] a hybrid approach that combines gas-phase clustering by explicit solvent molecules and solvation of the cluster by the dielectric continuum. In particular, two discrete water molecules were added to both the neutral and anionic species, adjacent to every single ionizable site in the polyprotic acid, as suggested by Adam.[31] (The optimized coordinates of all species are available in the Supporting Information.) This dihydrated moiety adopts a nearly planar eight-membered ring structure controlled by hydrogen bonds. The calculation of pk_i of a given acidic site in the acid AH makes use of the proton-transfer reaction[30,38]

$$HA(H_2O)_2 + OH^-(H_2O)_2 \rightarrow A^-(H_2O)_2 + H_2O(H_2O)_2$$

that leads to the following expression for pk_i at 298.15 K

$$pK_i = (\Delta G_{solv})/1.364 + 15.74$$

The ΔG_{gas} values were calculated with the DFT/PBE0/6−311+G(d,p) approach using Gaussian 03.[9] Free energies of solvation on gas-phase supermolecule geometries were estimated with the PCM method at the HF/6−31+G(d) level of theory using Gaussian 98 (in which the original PCM version and the related optimized UAHF radii are implemented).[46]

Of course, the clustered systems can be built in a variety of models. To overcome this difficulty, we relate the pk_i value calculated for each of our species to the pk_a calculated (and experimentally determined) for a simple reference system containing a similar functional group surrounded by an analogous hydrated cluster:

$$pk_i(\text{corrected}) = pk_i(\text{calc}) - [pk_a(\text{calc;ref}) - pk_a(\text{exp ;ref})]$$

These reference systems are benzoic acid (exp. pk_a 4.20)[47] and phenylacetic acid (exp. pk_a 4.36).[47] Therefore, because of the implications of all the structural and methodological assumptions, the relevance of the present study is not referred to the absolute quality of the calculated pk_is, which should best be viewed as order-of-magnitude estimates, but is restricted to analysis of their main features.

The use of the cluster-continuum method leads to the following estimates of the pk_is: 1.30 (enolic) and 3.64 (carboxymethyl) for **NH**; 2.16 (enolic), 4.84 (carboxymethyl), and 4.92 (carboxyl) for **HP**. Accordingly, in both compounds, the first deprotonation occurs predominantly from the enolic group. The second deprotonation involves the carboxymethyl site in **NH** while it involves either the carboxymethyl or the carboxyl site in **HP**. As expected, the calculated pk_is of the carboxymethyl and carboxyl dissociations resemble those of the simple related compounds. Instead, one particularly noteworthy point is the very strong acidic character of the enolic proton. The corresponding anionic structure is indeed strongly stabilized by extended resonance within the fluorenoid nucleus. This prediction is in agreement with the experimental data obtained for the pk_a of a pigment-related compound, 2.7−3.3 in 50% aqueous methanol.[5] Furthermore, it indicates that **NH** and **HP** should exist predominantly in anionic forms in water.

Another interesting aspect of the results is that the lowest pk_i differs from the other pk_is by more than 2 units. Thus, the p$K_{a,1}$ value of **NH** and **HP** should be very similar to their pk_i(enolic) and, therefore, approximately 1−2. Finally, it is

TABLE 2: Geometrical (distances in Å, angles in deg), Topological (electronic density and Laplacian of electronic density in a.u.), and Energetic (kcal mol^{-1}) Parameters of O−H···O Bridges[a]

	O−H	H···O	O···O	α(O−H···O)	ρ_{O-H}	$\nabla^2\rho_{O-H}$	$\rho_{H\cdots O}$	$\nabla^2\rho_{H\cdots O}$	E_{HB}
NH/A/nhb									
keto−enol	1.022	1.537	2.549	170.0	0.2966	−1.9830	0.0702	0.1477	−23.6
NH/A/hb									
keto−enol	1.013	1.570	2.572	169.2	0.3057	−2.0915	0.0640	0.1493	−22.33
keto-carboxymethyl	0.974	1.834	2.752	155.9	0.3508	−2.5157	0.0323	0.1128	−8.9
HP/A/nhb									
keto−enol	1.027	1.499	2.516	169.9	0.2911	−1.9119	0.0774	0.1517	−29.3
keto-carboxymethyl	0.984	1.691	2.646	106.4	0.3358	−2.3750	0.0469	0.1394	−14.6
HP/A/hb									
keto−enol	1.015	1.539	2.543	169.0	0.3027	−2.0529	0.0692	0.1551	−25.1
keto-carboxymethyl	0.972	1.860	2.771	154.8	0.3533	−2.5323	0.0304	0.1081	−8.2
keto-carboxylic	0.983	1.701	2.652	161.7	0.3371	−2.3878	0.0457	0.1378	−14.2

[a] The labels carboxymethyl and carboxylic stand for (side) carboxymethyl group and (central) carboxylic group, respectively.

worthwhile noting the much stronger acidity of **NH** and **HP** compared to that of 2-hydroxybenzaldehyde (pK_a = 8.38),[48] 3-hydroxycoumarin (7.2),[49] and 5-hydroxy-1,4-naphthoquinone (8.85),[50] all of these compounds bearing a carbonyl-enolic proton, phenol (9.99),[47] and a typical sunscreen such as *p*-aminobenzoic acid (4.8).[51] Again, this feature indicates that, upon entering the cell, the majority of the **NH** and **HP** molecules will dissociate into anions and protons that contribute to bacterial inhibition.

C. Absorption spectra. The UV−vis spectra of the hippopotamus's natural pigments **NH** and **HP** were obtained by Saikawa et al.[1] only in solution 0.2 M NaCl/0.2 M phosphate buffer, pH 6.1, where both neutral and anionic species should be present. In particular, **NH** shows absorption at λ_{max} (log ε) 511 nm (3.95), 418 (4.16), 271sh (4.29), 243 (4.73), and **HP** at λ_{max} (log ε) 530 nm (3.95), 411 (4.08), 270sh (4.31), 240 (4.72). Thus, the buffer solution of **NH** appears orange, while that of **HP** is red. A rigorous theoretical elucidation of the absorption spectra of these compounds, polyprotic with two (**NH**) or three (**HP**) different, dissociable protons and structurally multifaceted with various possible tautomer/conformers, is therefore a very difficult task.

Before discussion of the spectra, one important point must be stressed. The absorption spectra of **NH** and **HP** arise from $n\rightarrow\pi^*$ and $\pi\rightarrow\pi^*$ excitations. The solvatochromic effects on these excitations occurring in hydrogen-bonding solvents are very complex and may be positive or negative.[52−54] The standard TD-DFT/PCM calculations account for the electronic perturbations due to the intramolecular hydrogen bonds and the continuum solvation (bulk electrostatics) effects but neglect the specific perturbation of the intermolecular hydrogen bonds between solute and solvent. Various sophisticated formalisms, such as the Zeng−Hush−Reimers solvent shift (ZHR-SS) method,[53] could be used for better modeling the solvent effects. However, by taking into account that the relevance of the present study is restricted to analysis of the main features in the spectra of **NH** and **HP**, further computationally heavy calculations for a large number of neutral and anionic species were unpractical. On the other hand, from a qualitative standpoint, the influence of the intermolecular hydrogen bonds on the $n\rightarrow\pi^*$ and $\pi\rightarrow\pi^*$ excitations of the present compounds should be rather modest.

1. Reference Compounds. As a yardstick for the TD-DFT/PCM interpretation of the spectra of **NH** and **HP**, it was considered useful to check how such calculations account for the absorption spectra of some related simple molecules, 1,4:5,8-anthracenediquinone and juglone, i.e. 5-hydroxy-1,4-naphthoquinone, both neutral and anionic.

The electronic and magnetic circular dichroism spectra of 1,4:5,8-anthracenediquinone in dichloromethane solution present a very weak absorption at λ 450 nm, two weak absorptions at 360 and 330 nm, and two strong absorptions at 266 and 249 nm.[55] According to TD-DFT/PCM, the observed lowest energy feature is due to a very weak $n\rightarrow\pi^*$ transition (theory: λ 457 nm, oscillator strength f 0.00001, with the orientation of the transition moment perpendicular to the molecular plane). The lowest two $\pi\rightarrow\pi^*$ transitions are predicted at λ 352 nm (f 0.0066, short-axis polarized) and 351 nm (f 0.1562, long-axis polarized): they correspond to the second absorption region. The third absorption region arises from two strong $\pi\rightarrow\pi^*$ transitions (λ 275 nm, f 0.2672, short-axis polarized; λ 238 nm, f 0.4810, short-axis polarized). Incidentally, we mention that the present TD-DFT/PCM results provide a more accurate and complete assignment than that obtained by Fukuda et al.[55] with semiempirical CNDO/S calculations.

Juglone in chloroform solution exhibits absorption maxima at 429 nm (log ε 3.58), 337 nm (3.08), 251 nm (4.16).[56] According to TD-DFT/PCM results, the lowest band is due to the HOMO→LUMO π(benzenoid)→π^*(benzoquinoid) transition (λ 427 nm, f 0.1178, long-axis polarized). A very weak quinoid electron transfer $n\rightarrow\pi^*$, calculated at 434 nm, is hidden under the long wavelength tail of this band. The second band is due to another weak π(benzenoid)→π^*(benzoquinoid) transition (λ 348 nm, f 0.0144, short-axis polarized), and the third band to an intense π(quinoid)→π^*(benzoquinoid) transition (λ 257 nm, f 0.3331, short-axis polarized). A noteworthy point is that juglone is ionized at pH > 10 and turns from yellow to a deep pink color.[57] The absorption spectrum of a buffer solution 0.1 M NaOH shows two bands at 520 and 340 nm.[57] Thus, deprotonation of juglone, with its conversion in the juglone anion, produces a large bathochromic shift of the visible peak, which is correctly accounted for by the transitions given by TD-DFT/PCM: π(benzenoid)→π^*(benzoquinoid) (λ 553 nm, f 0.1293, long-axis polarized) and π(quinoid)→π^*(benzoquinoid) (λ 346 nm, f 0.0338, short-axis polarized).

Therefore, the theoretical formalism employed here provides a satisfactory description of the absorption spectra of 1,4:5,8-anthracenediquinone, neutral and anionic juglone. On this preliminary ground for the simple related molecules, the TD-DFT/PCM results should yield a consistent interpretation for the main features observed in the absorption spectra of the compounds **NH** and **HP**. On the other hand, it is worthwhile to mention that previous TD-DFT(PBE0)/PCM studies provided accurate reproductions of the experimental spectra of organic dyes.[58−61]

TABLE 3: Electronic Transitions of Norhipposudoric Species: Energies (nm) and Intensities (oscillator strength *f*) (calculated values for transitions with $f > 0.010$)[a,b]

NH(A)		**NH**(B)		**NH**(ph)$^-$		**NH**(cm)$^-$		**NH**$^{2-}$	
λ	f	λ	f	λ	f	λ	f	λ	f
566[c]	0.022	566[c]	0.022	523[c]	0.023	674[c]	0.002	507[c]	0.020
491	0.179	492	0.175	476	0.113	527	0.041	466	0.068
405	0.092	406	0.096	402	0.202	501	0.131	403	0.250
338	0.013	337	0.010	308	0.072	474	0.018	391	0.013
309	0.019	304	0.041	280	0.124	446	0.190	378	0.016
308	0.025	288	0.161	263	0.015	377	0.032	290	0.068
282	0.123	259	0.015	254	0.123	363	0.012	269	0.148
266	0.054	245	0.104	242	0.104	352	0.012	253	0.157
247	0.134	238	0.085	230	0.159	314	0.033	240	0.082
234	0.049	227	0.364	228	0.563	310	0.029	229	0.136
227	0.389	223	0.391	222	0.030	283	0.071	228	0.626
222	0.313	215	0.251	217	0.173	281	0.078		
215	0.265			215	0.128	253	0.100		
						239	0.316		
						234	0.045		
						233	0.033		
						224	0.039		
						222	0.328		
						219	0.224		
						215	0.211		

[a] Labels ph and cm correspond to phenolic and (side) carboxymethyl deprotonated units, respectively. [b] Experimental data in solution 0.2 M NaCl/0.2 M phosphate buffer, pH 6.1, ref:[1] λ_{max} (log ε) 511 (3.95), 418 (4.16), 271sh (4.29), 243 (4.73). [c] Electronic transition with dominant π(HOMO)$\rightarrow\pi$(LUMO)* character.

TABLE 4: Electronic Transitions of Hipposudoric Neutral and Anionic Species: Energies (nm) and Intensities (oscillator strength *f*) (calculated values for transitions with $f > 0.010$)[a,b]

HP(A)		**HP**(B)		**HP**(ph)$^-$		**HP**(cm)$^-$		**HP**(ca)$^-$	
λ	f	λ	f	λ	f	λ	f	λ	f
569[c]	0.021	553[c]	0.016	498[c]	0.014	690[c]	0.003	643[c]	0.138
479	0.132	492	0.104	465	0.028	553	0.061	598	0.026
408	0.110	420	0.136	426	0.025	526	0.047	438	0.049
371	0.021	380	0.027	406	0.243	462	0.235	411	0.079
317	0.020	302	0.019	393	0.042	411	0.017	396	0.081
283	0.090	289	0.127	379	0.010	398	0.023	371	0.013
281	0.048	279	0.035	310	0.050	370	0.039	356	0.034
257	0.237	254	0.022	281	0.035	305	0.021	304	0.029
240	0.042	251	0.232	279	0.017	291	0.149	297	0.023
232	0.022	234	0.235	274	0.161	259	0.020	293	0.135
231	0.362	228	0.232	257	0.101	254	0.155	269	0.063
230	0.027	218	0.176	251	0.076	249	0.188	268	0.024
219	0.124			237	0.131	234	0.252	257	0.016
218	0.111			236	0.012	232	0.079	246	0.056
				233	0.171	228	0.045	233	0.029
				231	0.083	226	0.242	229	0.095
				218	0.020			228	0.071
				217	0.021			226	0.286
				215	0.232			220	0.436

[a] Labels ph, cm, and ca correspond to phenolic, (side) carboxymethyl, and (central) carboxylic deprotonated units, respectively. [b] Experimental data in solution 0.1 M NaCl/0.2 M phosphate buffer, pH 6.1, ref:[1] λ_{max} (log ε) 530 (3.95), 411 (4.08), 270 sh (4.31), 240 (4.72). [c] Electronic transition with dominant π(HOMO)$\rightarrow\pi$(LUMO)* character.

2. Hippopotamus' Pigments. The TD-DFT/PCM results for all the most preferred neutral and deprotonated anionic forms of **NH** and **HP** are gathered in Tables 3−5. However, among all of the electronic transitions calculated, only the most intense ones (with $f > 0.010$) were reported in the tables. Furthermore, to allow for a direct appreciation of the absorption features and correlation with the experimental data, the UV−vis spectra were simulated using Gaussian functions with a full width at half-maximum (fwhm) of 0.20 eV for each individual optical peak. These computed spectra are displayed in Figures 6−8. Also, to illustrate the electronic excitations, the frontier molecular orbitals (MOs) of the lowest-energy tautomer/conformer of the neutral acids **NH**(A) and **HP**(A) are shown in Figures 9 and 10. As to the tautomeric effects, Tables 3 and 4 show that the excitation energies of **NH** and **HP** are only slightly sensitive to change from tautomer A to tautomer B. Given the complex electronic pattern, only an essential overview of the salient aspects (position, intensity, polarization, and nature) related to the neutral and anionic species of tautomer A is presented here.

From a descriptive standpoint, the **NH** and **HP** molecules incorporate a strong chromophoric system, the fluorenoid nucleus, with a laterally appended carboxymethyl group, whose semilocalized $n_O\rightarrow\pi^*_{CO}$ and $\pi_{CO}\rightarrow\pi^*_{CO}$ excitations should cause absorption at high energy (as a reference, placed below 210 nm in the case of pure acetic acid[62]). On the other hand, the formal introduction of the carboxyl substituent in the central

TABLE 5: Electronic Transitions of Hipposudoric Dianionic and Trianionic Species: Energies (nm) and Intensities (oscillator strength *f*) (calculated values for transitions with $f > 0.010$)[a,b]

HP(ph,cm)$^{2-}$		**HP**(ph,ca)$^{2-}$		**HP**(cm,ca)$^{2-}$		**HP**$^{3-}$	
λ	f	λ	f	λ	f	λ	f
502[c]	0.017	550[c]	0.159	628[c]	0.001	521[c]	0.126
455	0.025	530	0.022	589	0.164	503	0.032
424	0.058	408	0.054	523	0.025	405	0.051
409	0.146	399	0.068	403	0.075	396	0.116
394	0.015	358	0.098	395	0.150	338	0.082
383	0.052	313	0.054	360	0.023	291	0.059
382	0.041	291	0.054	317	0.056	287	0.034
362	0.011	285	0.108	315	0.015	273	0.102
340	0.015	266	0.021	296	0.015	270	0.040
298	0.021	259	0.014	285	0.127	250	0.036
276	0.016	253	0.032	251	0.572	244	0.121
268	0.049	246	0.059	241	0.068	236	0.150
263	0.290	238	0.186	231	0.124	228	0.398
261	0.023	231	0.016	230	0.377		
243	0.031	227	0.706	224	0.014		
237	0.219	222	0.070				
236	0.068	216	0.020				
224	0.017						

[a] Labels ph, cm, and ca correspond to phenolic, (side) carboxymethyl, and (central) carboxylic deprotonated units, respectively. [b] Experimental data in solution 0.1 M NaCl/0.2 M phosphate buffer, pH 6.1, ref:[1] λ_{max} (log ε) 530 (3.95), 411 (4.08), 270 sh (4.31), 240 (4.72). [c] Electronic transition with dominant π(HOMO)$\rightarrow\pi$(LUMO)* character.

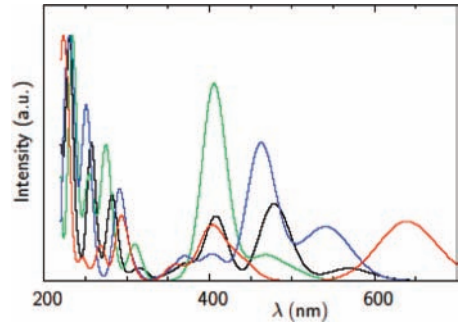

Figure 7. Computed UV−vis absorption spectra (simulated with fwhm = 0.20 eV) of **HP** species: neutral (black), enolic anion (green), side carboxymethyl anion (blue), and central carboxylic anion (red).

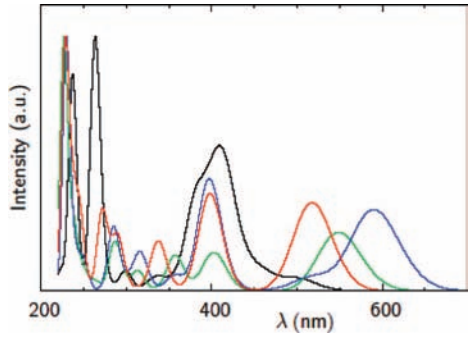

Figure 8. Computed UV−vis absorption spectra (simulated with fwhm = 0.20 eV) of **HP** species: enolic-carboxymethyl dianion (black), enolic-carboxylic dianion (green), carboxymethyl-carboxylic dianion (blue), and trianion (red).

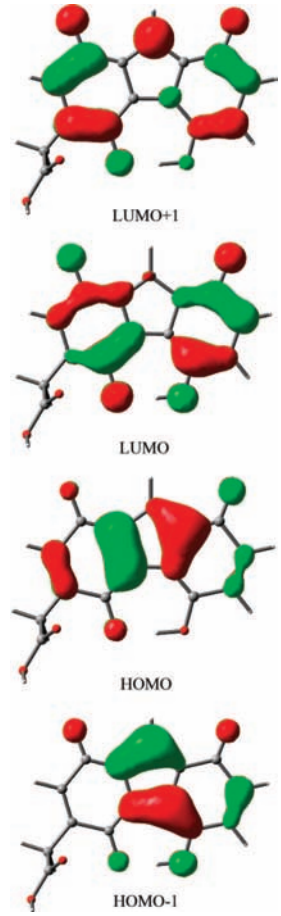

Figure 9. Frontier molecular orbitals of the lowest-energy tautomer/conformer of **NH**.

core of **NH** to give **HP** should mainly exert an inductive, bathochromic effect on the fluorenoid transitions, because steric hindrance keeps the carboxyl group from lying coplanar with the annelated rings (as observed for the related simple pair anthracene/9-anthracenecarboxylic acid[63]).

According to TD-DFT/PCM results (Tables 3 and 4), there is a close resemblance between the manifolds of electronic transitions of the two neutral compounds. Only transitions of $\pi\rightarrow\pi^*$ nature, which cause a redistribution of charge in the π bonding pattern of the fluorenoid moeity, provide a dominant contribution to the visible and mid-UV absorption regions of **NH** and **HP**. In particular, the lowest energy electronic excitations involve the frontier π MOs depicted in Figures 9 and 10. A noteworthy point is that the formal $\pi\rightarrow\pi^*$ diquinoid transitions of **NH** and **HP** exhibit a large bathochromic shift

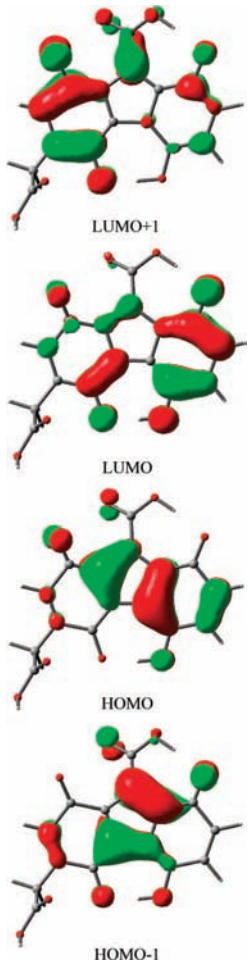

Figure 10. Frontier molecular orbitals of the lowest-energy tautomer/conformer of **HP**.

relative to the parent conjugated system 1,4:5,8-anthracenediquinone.[55] By reference to the neutral forms (Tables 3 and 4), the first two predicted electronic transitions (**NH**: 566 and 491 nm; **HP**: 569 and 479 nm; the longest wavelength, weakly allowed, short-axis polarized, and mainly due to the HOMO→LUMO excitation; the second, more intense, long-axis polarized, and ascribed to the HOMO-1→LUMO promotion) can be associated with the lowest-energy absorption in the visible region, peaked at 511 (**NH**) and 530 nm (**HP**), respectively. The relatively intense, long-axis polarized HOMO→LUMO+1 transition calculated at 405 (**NH**) and 408 nm (**HP**) is the principal contributor to the band centered at 418 (**NH**) and 411 nm (**HP**). An important aspect concerns the strong UV-absorption region with maxima observed at 271 and 243 nm (**NH**) and 270 and 240 nm (**HP**). It can mainly be associated with two peculiar $\pi \rightarrow \pi^*$ transitions, relatively intense and short-axis polarized. The first transition, calculated at 282 (**NH**) and 283 nm (**HP**), can be described as an intramolecular charge-transfer (CT) from the keto−enolic ring (the electron donor) to the quinoid ring (the electron acceptor), while the second transition, calculated at 247 (**NH**) and 257 nm (**HP**), involves the inverse CT process and resembles the feature observed at 251 nm for the related system juglone, mentioned above.

Notably, the formal, first deprotonation of **NH** and **HP** causes a large, but not monotonic displacement of the electronic transitions responsible for the absorption in the visible range, as shown by Tables 3 and 4 and Figures 6 and 7. Indeed, proton loss from the enolic group (the most acidic one, as shown above) is accompanied by a sizable hypsochromic shift, as a consequence of the increased energy gap within the original frontier π MOs. In contrast, dissociation involving a proton of the side carboxymethyl group or the central carboxyl group produces a large bathochromic shift, related to a net modification of the top π HOMOs that become largely concentrated over the COO^- fragment. On the whole, the more pronounced change is exhibited by the carboxymethyl anion. Further dissociation of **NH** and **HP** results in a subtle interplay of resonance and stereoelectronic factors that engender a complex movement of the transitions (Tables 4 and 5 and Figures 6−8). Also, the high negative charge favors a stronger interaction with protonic solvents (such as water) that appreciably affects the spectroscopic features. However, it is important to remark that the orange (red) color exhibited by the aqueous solution of **NH** (**HP**) is a manifestation mainly of their $\pi \rightarrow \pi^*$ diquinoid transitions.

As a final comment on the absorption spectra of **NH** and **HP**, it must be stressed that these natural pigments have been claimed to act as efficient sunscreens for the hippopotamus.[1] As can be seen from Figures 6−8, their aqueous solutions, containing both undissociated and dissociated forms, broadly absorb both in the UVA (320−400 nm) and UVB (280−320) regions of the spectrum. This prominent feature allows the hippopotamus, an animal subject to long exposure to sunlight, to prevent sunburn and reduce the harmful effects of solar radiation.[64] Furthermore, these natural sunscreen molecules, characterized by relatively strong intramolecular hydrogen bonds and also fit for forming intermolecular hydrogen bonds, should favor the biological thermoregulation of the hippopotamus by rapidly transferring the excess energy to their neighboring environment as thermal energy. Indeed, it has been shown that hydrogen-bonded species dissipate UV excitation energy more efficiently than nonbonded ones.[65,66]

4. Concluding Remarks

The molecular and electronic structures of **NH** and **HP**, the changeable pigments and potent antibiotics of *Hippopotamus amphibius*, have been studied with DFT calculations, performed at the PBE0/6−311+G(d,p) level. Among the five possible (keto−enol or bisquinoid) tautomers, two (referred to as A and B) have been predicted to have similar energies while being distinctly more stable than the others both in the gas phase and water. Because of the marked flexibility of the pendant (side) carboxymethyl and (central) carboxyl chains, these tautomers can adopt a multitude of conformations. However, consideration of the lowest-energy conformers allows for a reliable characterization of the compounds investigated, both in the undissociated and dissociated forms. A noteworthy structural feature concerns their intramolecular O−H···O hydrogen bonds. These have been analyzed in terms of the AIM topological properties of the electron density that manifest the remarkably high strength of the keto−enol bridge.

The site-specific microscopic dissociation constants of **NH** and **HP** in aqueous solution have been studied using the cluster-continuum model, a hybrid approach that combines gas-phase clustering by explicit solvent molecules and solvation of the cluster by the dielectric continuum (PCM method). Most interestingly, the enol group is predicted not only to be the most acidic of the various protonation sites of **NH** and **HP** but also to have an unexpectedly low pk_i. This finding is in accord with the experimental data for a pigment analogue and confirms the claimed acid strength of **NH** and **HP**.

The low-lying electronic excited states of both neutral and anionic **NH** and **HP** have been characterized in terms of the

main one-electron jumps in the fluorenoid moiety. The sizable hypsochromic shift in the visible range, which is caused by deprotonation in water, has also been accounted for by TD-DFT/PCM calculations. The orange (red) color of aqueous solutions of **NH** (**HP**) is a direct manifestation of $\pi \rightarrow \pi^*$ diquinoid transitions. The efficient sunscreen activity of **NH** and **HP** stems from their broad absorption in the UVA and UVB regions of the spectrum.

Supporting Information Available: Cartesian coordinates of all dihydrated neutral and anionic species involved in the pk_i calculations. This material is available free of charge via the Internet at http://pubs.acs.org.

Acknowledgment. V.G. thanks the Italian Ministero dell'Istruzione, dell'Università e della Ricerca. F.P. thanks the Graduate School of Engineering and the Global COE program of Tohoku University (Japan) for financial support.

References and Notes

(1) Saikawa, Y.; Hashimoto, K.; Nakata, M.; Yoshihara, M.; Nagai, K.; Ida, M.; Komiya, T. *Nature* **2004**, *429*, 363.
(2) Moriya, K.; Matsuura, M.; Saikawa, Y.; Hashimoto, K.; Uenishi, J.; Nakata, M.; Yamaguchi, A.; Sakamoto, K.; Akihisa, N.; Hirata, H. *Nippon Kagakkai Koen Yokushu* **2006**, *86*, 1314.
(3) Hashimoto, K.; Saikawa, Y.; Masaya, N. *Yuki Gosei Kagaku Kyokaishi* **2006**, *64*, 1251.
(4) Saikawa, Y.; Moriya, K.; Hashimoto, K.; Nakata, M. *Tetrahedron Lett.* **2006**, *47*, 2535.
(5) Hashimoto, K.; Saikawa, Y.; Nakata, M. *Pure Appl. Chem.* **2007**, *79*, 507.
(6) (a) Adamo, C.; Barone, V. *J. Chem. Phys.* **1999**, *110*, 6158. (b) Ernzerhof, M.; Scuseria, G. E. *J. Chem. Phys.* **1999**, *110*, 5029.
(7) Stratmann, R. E.; Scuseria, G. E.; Frisch, M. J. *J. Chem. Phys.* **1998**, *109*, 8218.
(8) Barone, V.; Cossi, M.; Tomasi, J. *J. Chem. Phys.* **1997**, *107*, 3210.
(9) Frisch, M. J.; Trucks, G. W.; Schlegel, H. B.; Scuseria, G. E.; Robb, M. A.; Cheeseman, J. R.; Montgomery, J. A.; Vreven, T.; Kudin, K. N.; Burant, J. C.; Millam, J. M.; Iyengar, S. S.; Tomasi, J.; Barone, V.; Mennucci, B.; Cossi, M.; Scalmani, G.; Rega, N.; Petersson, G. A.; Nakatsuji, H.; Hada, M.; Ehara, M.; Toyota, K.; Fukuda, R.; Hasegawa, J.; Ishida, M.; Nakajima, T.; Honda, Y. ; Kitao, O.; Nakai, H.; Klene, M.; Li, X.; Knox, J. E.; Hratchian, H. P.; Cross, J. B.; Bakken, V.; Adamo, C.; Jaramillo, J.; Gomperts, R.; Stratmann, R. E.; Yazyev, O.; Austin, A. J. ; Cammi, R.; Pomelli, C.; Ochterski, J. W.; Ayala, P. Y.; Morokuma, K.; Voth, G. A.; Salvador, P.; Dannenberg, J. J.; Zakrzewski, V. G.; Dapprich, S.; Daniels, A. D.; Strain, M. C.; Farkas, O.; Malick, D. K.; Rabuck, A. D.; Raghavachari, K.; Foresman, J. B.; Ortiz, J. V.; Cui, Q.; Baboul, A. G.; Clifford, S.; Cioslowski, J.; Stefanov, B. B.; Liu, G.; Liashenko, A.; Piskorz, P.; Komaroni, I.; Martin, R. L.; Fox, D. J.; Keith, T.; Al-Laham, M. A.; Peng, C. Y.; Nanayakkara, A.; Challacombe, M.; Gill, P. M. W.; Johnson, B.; Chen, W.; Wong, M. W.; Gonzalez, C.; Pople, J. A. Gaussian 03, Revision D.01, Gaussian Inc.; Wallingford, CT, 2004.
(10) Hodgson, D. J.; Asplund, R. O. *Acta Crystallogr.* **1991**, *C47*, 1986.
(11) Okabe, N.; Kohyama, Y. *Acta Crystallogr.* **1995**, *C51*, 761.
(12) (a) Peng, C.; Ayala, P. Y.; Schlegel, H. B.; Frisch, M. J. *J. Comput. Chem.* **1996**, *17*, 49. (b) Peng, C.; Schlegel, H. B. *Isr. J. Chem.* **1994**, *33*, 449.
(13) (a) Jeffrey, G. A.; Saenger, W. *Hydrogen Bonding in Biological Structures*; Springer-Verlag: Berlin, 1991. (b) Garcia-Viloca, M.; Lafont, A. G.; Lluch, J. M. *J. Am. Chem. Soc.* **1997**, *118*, 1081. (c) Schiøtt, B.; Iversen, B. B.; Madsen, G. K. H.; Bruice, T. C. *J. Am. Chem. Soc.* **1998**, *120*, 12117.
(14) Terada, H. *Environ. Health Perspect.* **1990**, *87*, 213.
(15) Lipkowski, P.; Koll, A.; Karpfen, A.; Wolschann, P. *Chem. Phys. Lett.* **2002**, *360*, 256.
(16) Estacio, S. G.; Cabral do Counta, P.; Costa Cabral, B. J.; Minas Da Piedade, M. E.; Martinho Simoes, J. A. *J. Phys. Chem. A* **2004**, *108*, 10834.
(17) Deev, V.; Collins, M. A. *J. Chem. Phys.* **2005**, *122*, 154102.
(18) Musin, R. N.; Mariam, Y. H. *J. Phys. Org. Chem.* **2006**, *19*, 425.
(19) Roy, D.; Sunoj, R. B. *J. Phys. Chem. A* **2006**, *110*, 5942.
(20) Deshmukh, M. M.; Gadre, S. R.; Bartolotti, L. J. *J. Phys. Chem. A* **2006**, *110*, 12519.
(21) Filarowski, A.; Majerz, I. *J. Phys. Chem. A* **2008**, *112*, 3119.
(22) Bader, R. F. W. *Atoms in Molecules: a Quantum Theory*; Clarendon Press: Oxford, 1990.
(23) Abramov, Y. A. *Acta Crystallogr., Sect A: Found. Crystallogr.* **1997**, *53*, 264.
(24) Espinosa, E.; Molins, E.; Lecomte, C. *Chem. Phys. Lett.* **1998**, *285*, 170.
(25) Bader, R. F. W.; MacDougall, P. J.; Lau, C. D. H. *J. Am. Chem. Soc.* **1984**, *106*, 1594.
(26) Wojtulewski, S.; Grabowski, S. J. *J. Mol. Struct. (THEOCHEM)* **2003**, *621*, 285.
(27) Trendafilova, N.; Bauer, G.; Mihaylov, T. *Chem. Phys.* **2004**, *302*, 95.
(28) Szakács, Z.; Noszál, B. *J. Math. Chem.* **1999**, *26*, 139.
(29) Jang, Y. H.; Goddard, W. A., III.; Noyes, K. T.; Sowers, L. C.; Hwang, S.; Chung, D. S. *Chem. Res. Toxicol.* **2002**, *15*, 1023.
(30) Pliego, J. R., Jr.; Riveros, J. M. *J. Phys. Chem. A* **2002**, *106*, 7434.
(31) Adam, K. R. *J. Phys. Chem. A* **2002**, *106*, 11963.
(32) Klamt, A.; Eckert, F.; Diedenhofen, M.; Beck, M. E. *J. Phys. Chem. A* **2003**, *107*, 9380.
(33) Saracino, G. A. A.; Improta, R.; Barone, V. *Chem. Phys. Lett.* **2003**, *373*, 411.
(34) De Abreu, H. A.; De Almeida, W. B.; Duarte, H. A. *Chem. Phys. Lett.* **2004**, *383*, 47.
(35) Canle, M. L.; Ramos, D. R.; Santaballa, J. A. *Chem. Phys. Lett.* **2006**, *417*, 28.
(36) Kelly, C. P.; Cramer, C. J.; Truhlar, D. G. *J. Phys. Chem. A* **2006**, *110*, 2493.
(37) da Silva, G.; Kennedy, E. M.; Dlugogorski, B. Z. *J. Phys. Chem. A* **2006**, *110*, 11371.
(38) Jia, Z.; Du, D.; Zhou, Z.; Zhang, A.; Hou, R. *Chem. Phys. Lett.* **2007**, *439*, 374.
(39) Perpète, E. A.; Ciofini, I.; Adamo, C. *J. Phys. Chem. A* **2008**, *112*, 794.
(40) Tomasi, J.; Persico, M. *Chem. Rev.* **1994**, *94*, 2027.
(41) Cramer, C.; Truhlar, D. G. *Chem. Rev.* **1999**, *99*, 2161.
(42) Orozco, M.; Luque, F. J. *Chem. Rev.* **2000**, *100*, 4187.
(43) Tomasi, J.; Mennucci, B.; Cammi, R. *Chem. Rev.* **2005**, *105*, 2999.
(44) Rega, N.; Scalmani, G.; Barone, V. *J. Comput. Chem.* **2003**, *24*, 669.
(45) Suci, M.; Jing, M. *J. Phys. Chem. B* **2007**, *111*, 4128.
(46) Frisch, M. J.; Trucks, G. W.; Schlegel, H. B.; Scuseria, G. E.; Robb, M. A.; Cheeseman, J. R.; Zakrzewski, V. G.; Montgomery, J. A., Jr.; Stratmann, R. E.; Burant, J. C.; Dapprich, S.; Millam, J. M.; Daniels, A. D.; Kudin, K. N.; Strain, M. C.; Farkas, O.; Tomasi, J.; Barone, V.; Cossi, M.; Cammi, R.; Mennucci, B.; Pomelli, C.; Adamo, C.; Clifford, S.; Ochterski, J.; Petersson, G. A.; Ayala, P. Y.; Cui, Q.; Morokuma, K.; Malick, D. K.; Rabuck, A. D.; Raghavachari, K.; Foresman, J. B.; Cioslowski, J.; Ortiz, J. V.; Stefanov, B. B.; Liu, G.; Liashenko, A.; Piskorz, P.; Komaromi, I.; Gomperts, R.; Martin, R. L.; Fox, D. J.; Keith, T.; Al-Laham, M. A.; Peng, C. Y.; Nanayakkara, A.; Gonzalez, C.; Challacombe, M.; Gill, P. M. W.; Johnson, B. G.; Chen, W.; Wong, M. W.; Andres, J. L.; Head-Gordon, M.; Replogle, E. S.; Pople, J. A. Gaussian 98, revision A.6; Gaussian, Inc.: Pittsburgh, PA, 1998.
(47) Rappoport, Z. *CRC Handbook of Tables for Organic Compound Identification*; The Chemical Rubber Co.: Cleveland, OH, 1967.
(48) Rochester, C. H.; Wilson, D. N. *J. Chem. Soc., Faraday Trans. 2* **1976**, 2930.
(49) Wolfbeis, O. S. *Z. Phys. Chem.* **1981**, *125*, 15.
(50) Palit, D. K.; Mukherjee, T.; Mittal, J. P. *J. Indian Chem. Soc.* **1986**, *63*, 35.
(51) Terada, H. *Chem. Pharmacol. Bull.* **1972**, *20*, 765.
(52) Reichardt, C. *Chem. Rev.* **1994**, *94*, 2319.
(53) Hush, N. S.; Reimers, J. R. *Chem. Rev.* **2000**, *100*, 775.
(54) Suci, M.; Jing, M. *J. Phys. Chem. B* **2008**, *112*, 4313.
(55) Fukuda, M.; Tajiri, A.; Oda, M.; Hatano, M. *Bull. Chem. Soc. Jpn.* **1983**, *56*, 592.
(56) Singh, I.; Ogata, R. T.; Moore, R. E.; Chang, C. W. J.; Scheuer, P. J. *Tetrahedron* **1968**, *24*, 6053.
(57) Górski, Z.; Rolewski, P.; Sławińskia, D.; Sławiński, J. *Electron. J. Pol. Agric. Univ.* **2004**, *7*, 1.
(58) Ciofini, I.; Lainé, P. P.; Bediuni, F.; Adamo, C. *J. Am. Chem. Soc.* **2004**, *126*, 10763.
(59) Jacquemin, D.; Preat, J.; Wathelet, V.; Fontaine, M.; Perpète, E. A. *J. Am. Chem. Soc.* **2006**, *128*, 2072.
(60) Improta, R.; Barone, V.; Santoro, F. *Angew. Chem., Int. Ed.* **2007**, *46*, 405.
(61) Jacquemin, D.; Perpète, E. A.; Scuseria, G. E.; Ciofini, I.; Adamo, C. *J. Chem. Theory Comput.* **2008**, *4*, 123.
(62) (a) Barnes, E. E.; Simpson, W. T. *J. Chem. Phys.* **1963**, *39*, 670. (b) Bell, S.; Ng, T. L.; Walsh, A. D. *J. Chem. Soc., Faraday Trans. 2* **1975**, 393.
(63) (a) Friedrich, D. M.; Mathieu, R.; Albrecht, A. C. *J. Mol. Spectrosc.* **1974**, *51*, 166. (b) Werner, T. C.; Hercules, D. M. *J. Phys. Chem.* **1969**, *73*, 2005.
(64) Eltringham, S. K. The Hippos; T&AD Poyser: London, 1999.
(65) Conde, F. R.; Churio, M. S.; Previtali, C. M. *Photochem. Photobiol. Sci.* **2004**, *3*, 960.
(66) Schultz, E.; Samoylova, E.; Radloff, W.; Hertel, I. V.; Sobolewski, A. L.; Domcke, W. *Science* **2004**, *306*, 1765.

JP809138S